JOURNAL OF GUIDANCE, CONTROL, AND DYNAMICS
Vol. 29, No. 2, March–April 2006

Optimal Control of an Aircraft-Towed Flexible Cable System

Paul Williams,* Daniel Sgarioto,† and Pavel Trivailo‡
Royal Melbourne Institute of Technology University, Melbourne, Victoria 3083, Australia

The control of an aerial-towed flexible cable system for precision rendezvous and snatch pickup of payloads is considered. In past studies of related systems, optimal trajectories have been determined assuming that the cable remains straight. However, aerodynamic drag and deployment forces can cause bowing of the cable that can significantly alter the position of the cable tip relative to the aircraft. To account for this, the cable is modeled using lumped masses connected via rigid links. Multiple rendezvous sequences using only cable winch control and including features such as collision avoidance and variable winds are solved by multiple-phase direct transcription methods. Numerical results show that for some multiple rendezvous scenarios it is necessary to use the cable lateral dynamics and swing motion to avoid impact with elevated terrain. The effect of different wind speeds and directions are also studied.

Introduction

TOWED-CABLE body systems have found practical use in both underwater and aerial applications.[1–4] Aerial-towed cable systems have been proposed for a number of applications, most of which require accurate positioning of the cable tip. In particular deployment/retrieval of payloads could be achieved by towing a cable in a circular path to achieve near stationary motion of the cable tip.[5–7] An early application of aerial cable systems for picking up payloads was developed by Lytle Adams and Boeing engineers in 1928. The idea, which later became known as air pick up, used a Stinson aircraft with a deployed boom to pick up a cargo container that was attached to a rope connected between two poles (14 ft high and 20 ft wide). A hook at the end of the boom engaged the rope, and additional rope was deployed via a constant tension reel to absorb the shock. The rope and payload were subsequently reeled back into the aircraft. This method was used to deliver express mail in the United States during the 1930–1950 period by All American Aviation.[8] However, this application requires the aircraft to fly close to the ground, and guidance for pickup must be provided by the pilot. The disadvantage of this method is that the hook used to engage the rope is located to the rear of the pilot. An alternative method that was employed to extract crew from remote locations was the Fulton skyhook. This method used a "skyanchor" on the nose boom of the aircraft to hook onto a line hoisted by a helium balloon.[9] A similar concept to the air pickup maneuver was investigated for a more advanced system by Jun et al.,[10] who studied optimal guidance maneuvers using a towed vehicle with active control surfaces to guide the cable tip to a stationary ground target. Jun et al.[10] designed the controller using a linear quadratic digital regulator and ignored the coupling between the cable dynamics and endbody control.

A variety of studies of aircraft-towed-body systems have been presented in the literature. Huffman and Genin[11] used a continuum representation of an extensible cable to study the dynamics of a sphere towed from an aircraft at constant speed. Phillips[12] developed a theory to show that transverse waves propagated upwind on the cable are damped, but waves propagated downwind are only slightly damped if the wave speed exceeds the wind speed. Genin et al.[13] considered the coupling between the transverse cable motion and longitudinal modes of vibration of a towed cable. They demonstrated that the coupling is caused by several interactions related to the change in the average tension along the cable, geometric nonlinearities, and centripetal acceleration effects. Norris and Andrisani[14] determined equilibrium configurations of a C-141 cargo aircraft towing a modified F-106 fighter. The continuous partial differential equations representing the cable were integrated numerically to determine the cable shape. Reasonably good agreement between theory and flight tests was obtained.

The stability of towed aerial systems has been studied by Nakagawa and Obata[15] using an assumed mode approach for the cable vibrations. The cable was assumed flexible, but inextensible. Only two-dimensional motion was considered, and the towing vehicle was assumed to be flying straight at relatively high speed. Numerical results suggest that a towed sphere can become unstable by way of cable flutter if the size of the towed body (sphere) is small. Etkin[16] also studied the stability of towed aerial bodies, but considered the effect of cable extensibility. Etkin demonstrated that towed bodies subjected only to aerodynamic drag are not unstable, but bodies that provide lift and other forces can become unstable. The instability can be eliminated by proper positioning of the cable attachment point on the towed vehicle.

Cochran et al.[17] considered active control of the towed vehicle. Numerical simulations of the controller were performed using a variable-length inextensible cable model. Cable flexibility was treated using a lumped mass representation, and changes in cable length were accommodated by varying the length of the link closest to the aircraft. The towed vehicle was modeled as a rigid body whose motion was controlled by aerodynamic control surfaces (elevators, rudders, ailerons). Active control of the towed vehicle has also been considered by Henderson et al.[18] Bourmistrov et al.[19] developed a nonlinear controller for a towed body, explicitly accounting for the cable tension. The controller was based on an inversion of the dynamic and kinematic equations of motion for the towed body. More recently, the application of towed systems for low-altitude atmospheric research has been considered by Quisenberry and Arena.[20] Control of the towed vehicle for tracking ocean waves was implemented by measuring the height of the ocean waves via a radar altimeter. A proportional–derivative controller, implementing corrections to the wing angle on the towed vehicle, was used to track the ocean waves. Other related studies of towed aerial systems have focused on the stability and control of cables towed in a circular path.[21–23] The control of cable deployment/retrieval for rendezvousing with ground targets was examined by Trivailo et al.[24] assuming a straight, rigid cable. No previous work has specifically dealt with the control of cable deployment for achieving rendezvous taking into account cable flexibility. This is one of the aims of this paper.

Received 15 October 2004; revision received 23 March 2005; accepted for publication 29 March 2005.

*Research Fellow, P.O. Box 71, School of Aerospace, Mechanical and Manufacturing Engineering, Bundoora; paul.williams@rmit.edu.au. Member AIAA.

†Ph.D. Candidate, P.O. Box 71, School of Aerospace, Mechanical and Manufacturing Engineering, Bundoora.

‡Professor, P.O. Box 71, School of Aerospace, Mechanical and Manufacturing Engineering, Bundoora; trivailo@rmit.edu.au.

The purpose of this paper is to examine the performance of a snatch payload pickup system using a guidance algorithm designed via nonlinear optimal control. Instead of relying on aerodynamic control surfaces on the towed vehicle to provide guidance, it is proposed to perform guidance by only manipulating the length of deployed cable. It is desirable to control the length of deployed cable directly, as opposed to using tension control or control surfaces on the towed vehicle, because of uncertainties in estimating the cable tension at the towed vehicle. Furthermore, in this paper we consider more complex multiple-snatch scenarios incorporating terrain avoidance. Minimum reel acceleration trajectories are determined numerically using direct transcription methods.

Dynamic Model

Two modeling approaches have been used to model complex cable dynamics in the literature: 1) continuum models[25–29] and 2) lumped mass models.[30–35] The approaches have been compared,[36] and although it is believed that the continuum model provides the most accurate representation of the cable, the lumped mass model is the most versatile and simplest to program. We have selected a lumped mass model for the cable, represented by a set of generalized coordinates to minimize the number of state variables describing the system. This is an important consideration when direct transcription techniques are applied to obtain optimal trajectories if the computational requirements are to be reasonable.

The aircraft–cable system is modeled by first assuming that the motion of the aircraft is two dimensional and prescribed by accelerations $\ddot{x}$ and $\ddot{h}$ in the x and y directions, respectively, as shown in Fig. 1. The cable is modeled using a lumped parameter approach, which concentrates inertial and external forces to point mass elements articulated by frictionless hinges. In most of the scenarios studied in this paper, the cable is not expected to bend significantly, and hence, the number of point elements need not be very large. Furthermore, because the cable is constructed with a strong material, its longitudinal stretching may be neglected as a first approximation. This allows the cable segments to be described with rigid-link elements. A representation of the model for an arbitrary number of point mass elements n is shown in Fig. 1. The equations of motion are derived for the general case of n elements, but this is achieved by explicitly determining the equations of motion for the case when $n=4$. Hence, throughout this section the case when $n=4$ is used for illustrative purposes. A planar model of the cable has been selected for this study. We have ignored any possible lateral motion of the cable due to asymmetric aerodynamic loading on the cable[37] or lateral motion that could be induced by other phenomena such as vortex shedding.[38] Our choice of model and generalized coordinates is based primarily on its applicability to solving the optimal control problem considered later in this paper. We have found that convergence of the nonlinear programming problem is generally enhanced by eliminating the non-working tension forces and using angular orientations for the cable segments rather than Cartesian coordinates.

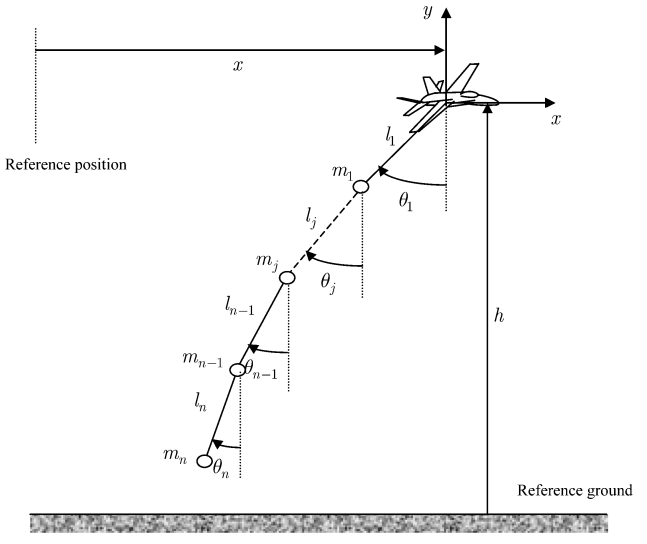

Fig. 1 Aircraft cable pickup system model.

The equations of motion are derived using Kane's equations (see Ref. 39), which allow the elimination of nonworking constraint forces without the lengthy process of differentiating kinetic energy expressions involved in Lagrange's equations. The generalized coordinates are selected as the rotation angles of the cable segments, θ_j, $j=1,\ldots,n$. The cable is allowed to deploy/retract by prescribing the reel acceleration $\ddot{l}_1(t)$ at the aircraft end. This is preferable to allowing each cable segment to change in length. This approach is similar to that used by Cochran et al.[17] In the model, large changes in length that would require discontinuities in the number of deployed masses are avoided, and cable deployment is simulated by adjusting the length of the first link l_1. All other links are assumed to remain constant in length, so that $l_1=l_1(t)$, $l_2=l_3=l_j=\cdots=l_n=l=\text{const}$. For simplicity, it is assumed that all constant length links have the same length l.

The inertial positions of the four-point masses relative to the reference axes may be written in terms of the generalized coordinates as

$$\boldsymbol{r}_1 = [x(t) - l_1(t)\sin\theta_1(t)]\boldsymbol{i} + [h(t) - l_1(t)\cos\theta_1(t)]\boldsymbol{j} \tag{1}$$

$$\boldsymbol{r}_2 = \boldsymbol{r}_1 - l\sin\theta_2(t)\boldsymbol{i} - l\cos\theta_2(t)\boldsymbol{j} \tag{2}$$

$$\boldsymbol{r}_j = \boldsymbol{r}_{j-1} - l\sin\theta_j(t)\boldsymbol{i} - l\cos\theta_j(t)\boldsymbol{j} \tag{3}$$

$$\boldsymbol{r}_n = \boldsymbol{r}_{n-1} - l\sin\theta_n(t)\boldsymbol{i} - l\cos\theta_n(t)\boldsymbol{j} \tag{4}$$

where $\boldsymbol{i}$ and $\boldsymbol{j}$ are unit vectors in the x and y directions, respectively.

The corresponding velocities are obtained by differentiating Eqs. (1–4),

$$\boldsymbol{v}_1 = [\dot{x}(t) - \dot{l}_1(t)\sin\theta_1(t) - l_1(t)\dot{\theta}_1(t)\cos\theta_1(t)]\boldsymbol{i} + [\dot{h}(t) - \dot{l}_1(t)\cos\theta_1(t) + l_1(t)\dot{\theta}_1(t)\sin\theta_1(t)]\boldsymbol{j} \tag{5}$$

$$\boldsymbol{v}_2 = \boldsymbol{v}_1 - l\dot{\theta}_2(t)\cos\theta_2(t)\boldsymbol{i} + l\dot{\theta}_2(t)\sin\theta_2(t)\boldsymbol{j} \tag{6}$$

$$\boldsymbol{v}_j = \boldsymbol{v}_{j-1} - l\dot{\theta}_j(t)\cos\theta_j(t)\boldsymbol{i} + l\dot{\theta}_j(t)\sin\theta_j(t)\boldsymbol{j} \tag{7}$$

$$\boldsymbol{v}_n = \boldsymbol{v}_{n-1} - l\dot{\theta}_n(t)\cos\theta_n(t)\boldsymbol{i} + l\dot{\theta}_n(t)\sin\theta_n(t)\boldsymbol{j} \tag{8}$$

The partial velocities are obtained as follows:

$$\frac{\partial \boldsymbol{v}_1}{\partial \dot{\theta}_1} = -l_1(t)\cos\theta_1(t)\boldsymbol{i} + l_1(t)\sin\theta_1(t)\boldsymbol{j} \tag{9}$$

$$\frac{\partial \boldsymbol{v}_1}{\partial \dot{\theta}_2} = \frac{\partial \boldsymbol{v}_1}{\partial \dot{\theta}_j} = 0, \qquad j=2,\ldots,n \tag{10}$$

$$\frac{\partial \boldsymbol{v}_2}{\partial \dot{\theta}_1} = \frac{\partial \boldsymbol{v}_1}{\partial \dot{\theta}_1} \tag{11}$$

$$\frac{\partial \boldsymbol{v}_2}{\partial \dot{\theta}_2} = -l\cos\theta_2(t)\boldsymbol{i} + l\sin\theta_2(t)\boldsymbol{j} \tag{12}$$

$$\frac{\partial \boldsymbol{v}_2}{\partial \dot{\theta}_3} = \frac{\partial \boldsymbol{v}_2}{\partial \dot{\theta}_j} = 0, \qquad j=3,\ldots,n \tag{13}$$

In general, we have

$$\frac{\partial \boldsymbol{v}_k}{\partial \dot{\theta}_j} = \begin{cases} \dfrac{\partial \boldsymbol{v}_j}{\partial \dot{\theta}_j}, & k \geq j \\ 0, & k < j \end{cases} \tag{14}$$

$$\frac{\partial \boldsymbol{v}_j}{\partial \dot{\theta}_j} = -l\cos\theta_j(t)\boldsymbol{i} + l\sin\theta_j(t)\boldsymbol{j}, \qquad j=2,\ldots,n \tag{15}$$

The accelerations are

$$\begin{aligned}\boldsymbol{a}_1 &= [\ddot{x}(t) - \ddot{l}_1(t)\sin\theta_1(t) - 2\dot{l}_1(t)\dot{\theta}_1(t)\cos\theta_1(t)\\ &\quad - l_1(t)\ddot{\theta}_1(t)\cos\theta_1(t) + l_1(t)\dot{\theta}_1^2(t)\sin\theta_1(t)]\boldsymbol{i}\\ &\quad + [\ddot{h}(t) - \ddot{l}_1(t)\cos\theta_1(t) + 2\dot{l}_1(t)\dot{\theta}_1(t)\sin\theta_1(t)\\ &\quad + l_1(t)\ddot{\theta}_1(t)\sin\theta_1(t) + l_1(t)\dot{\theta}_1^2(t)\cos\theta_1(t)]\boldsymbol{j} \qquad (16)\end{aligned}$$

$$\begin{aligned}\boldsymbol{a}_2 &= \boldsymbol{a}_1 + \left[l\dot{\theta}_2^2(t)\sin\theta_2(t) - l\ddot{\theta}_2(t)\cos\theta_2(t)\right]\boldsymbol{i}\\ &\quad + \left[l\dot{\theta}_2^2(t)\cos\theta_2(t) + l\ddot{\theta}_2(t)\sin\theta_2(t)\right]\boldsymbol{j} \qquad (17)\end{aligned}$$

$$\begin{aligned}\boldsymbol{a}_j &= \boldsymbol{a}_{j-1} + \left[l\dot{\theta}_j^2(t)\sin\theta_j(t) - l\ddot{\theta}_j(t)\cos\theta_j(t)\right]\boldsymbol{i}\\ &\quad + \left[l\dot{\theta}_j^2(t)\cos\theta_j(t) + l\ddot{\theta}_j(t)\sin\theta_j(t)\right]\boldsymbol{j} \qquad (18)\end{aligned}$$

$$\begin{aligned}\boldsymbol{a}_n &= \boldsymbol{a}_{n-1} + \left[l\dot{\theta}_n^2(t)\sin\theta_n(t) - l\ddot{\theta}_n(t)\cos\theta_n(t)\right]\boldsymbol{i}\\ &\quad + \left[l\dot{\theta}_n^2(t)\cos\theta_n(t) + l\ddot{\theta}_n(t)\sin\theta_n(t)\right]\boldsymbol{j} \qquad (19)\end{aligned}$$

Kane's equations for the multibody system are obtained as

$$F_{q_j}^* + F_{q_j} = 0, \qquad j = 1, \ldots, n \qquad (20)$$

where $F_{q_j}^*$ are the generalized inertia forces

$$F_{q_j}^* = \sum_{i=1}^{n} -m_i\boldsymbol{a}_i \cdot \frac{\partial \boldsymbol{v}_i}{\partial \dot{q}_j}, \qquad j = 1, \ldots, n \qquad (21)$$

F_{q_j} are the generalized active forces

$$F_{q_j} = \sum_{i=1}^{n} \boldsymbol{F}_i \cdot \frac{\partial \boldsymbol{v}_i}{\partial \dot{q}_j}, \qquad j = 1, \ldots, n \qquad (22)$$

and $\boldsymbol{F}$ is the vector of external forces.

Generalized Inertia Forces

The inertia forces are calculated as follows (for $n = 4$):

$$\begin{aligned}F_{\theta_1}^* &= -m_1\boldsymbol{a}_1 \cdot \frac{\partial \boldsymbol{v}_1}{\partial \dot{\theta}_1} - m_2\boldsymbol{a}_2 \cdot \frac{\partial \boldsymbol{v}_2}{\partial \dot{\theta}_1} - m_3\boldsymbol{a}_3 \cdot \frac{\partial \boldsymbol{v}_3}{\partial \dot{\theta}_1} - m_4\boldsymbol{a}_4 \cdot \frac{\partial \boldsymbol{v}_4}{\partial \dot{\theta}_1}\\ &= -(m_1\boldsymbol{a}_1 + m_2\boldsymbol{a}_2 + m_3\boldsymbol{a}_3 + m_4\boldsymbol{a}_4) \cdot \frac{\partial \boldsymbol{v}_1}{\partial \dot{\theta}_1}\\ &= (m_1 + m_2 + m_3 + m_4)l_1(t)[\ddot{x}(t)\cos\theta_1(t) - \ddot{h}(t)\sin\theta_1(t)\\ &\quad - 2\dot{l}_1(t)\dot{\theta}_1(t) - l_1(t)\ddot{\theta}_1(t)] + (m_2 + m_3 + m_4)\\ &\quad \times l l_1(t)\left\{\dot{\theta}_2^2(t)\sin[\theta_2(t) - \theta_1(t)] - \ddot{\theta}_2(t)\cos[\theta_2(t) - \theta_1(t)]\right\}\\ &\quad + (m_3 + m_4)l l_1(t)\left\{\dot{\theta}_3^2(t)\sin[\theta_3(t) - \theta_1(t)]\right.\\ &\quad \left. - \ddot{\theta}_3(t)\cos[\theta_3(t) - \theta_1(t)]\right\} + m_4 l l_1(t)\left\{\dot{\theta}_4^2(t)\sin[\theta_4(t)\right.\\ &\quad \left. - \theta_1(t)] - \ddot{\theta}_4(t)\cos[\theta_4(t) - \theta_1(t)]\right\} \qquad (23)\end{aligned}$$

$$\begin{aligned}F_{\theta_2}^* &= -m_1\boldsymbol{a}_1 \cdot \frac{\partial \boldsymbol{v}_1}{\partial \dot{\theta}_2} - m_2\boldsymbol{a}_2 \cdot \frac{\partial \boldsymbol{v}_2}{\partial \dot{\theta}_2} - m_3\boldsymbol{a}_3 \cdot \frac{\partial \boldsymbol{v}_3}{\partial \dot{\theta}_2} - m_4\boldsymbol{a}_4 \cdot \frac{\partial \boldsymbol{v}_4}{\partial \dot{\theta}_2}\\ &= -(m_2\boldsymbol{a}_2 + m_3\boldsymbol{a}_3 + m_4\boldsymbol{a}_4) \cdot \frac{\partial \boldsymbol{v}_2}{\partial \dot{\theta}_2}\\ &= (m_2 + m_3 + m_4)l\{\ddot{x}(t)\cos\theta_2(t) - \ddot{h}(t)\sin\theta_2(t)\\ &\quad + \ddot{l}_1(t)\sin[\theta_2(t) - \theta_1(t)] - [2\dot{l}_1(t)\dot{\theta}_1(t) + l_1(t)\ddot{\theta}_1(t)]\\ &\quad \times \cos[\theta_2(t) - \theta_1(t)] - l_1(t)\dot{\theta}_1^2(t)\sin[\theta_2(t) - \theta_1(t)]\}\\ &\quad - (m_2 + m_3 + m_4)l^2\ddot{\theta}_2(t) + (m_3 + m_4)l^2\left\{\dot{\theta}_3^2(t)\sin[\theta_3(t)\right.\\ &\quad \left. - \theta_2(t)] - \ddot{\theta}_3(t)\cos[\theta_3(t) - \theta_2(t)]\right\} + m_4 l^2\left\{\dot{\theta}_4^2(t)\sin[\theta_4(t)\right.\\ &\quad \left. - \theta_2(t)] - \ddot{\theta}_4(t)\cos[\theta_4(t) - \theta_2(t)]\right\} \qquad (24)\end{aligned}$$

$$\begin{aligned}F_{\theta_3}^* &= -m_1\boldsymbol{a}_1 \cdot \frac{\partial \boldsymbol{v}_1}{\partial \dot{\theta}_3} - m_2\boldsymbol{a}_2 \cdot \frac{\partial \boldsymbol{v}_2}{\partial \dot{\theta}_3} - m_3\boldsymbol{a}_3 \cdot \frac{\partial \boldsymbol{v}_3}{\partial \dot{\theta}_3} - m_4\boldsymbol{a}_4 \cdot \frac{\partial \boldsymbol{v}_4}{\partial \dot{\theta}_3}\\ &= -(m_3\boldsymbol{a}_3 + m_4\boldsymbol{a}_4) \cdot \frac{\partial \boldsymbol{v}_3}{\partial \dot{\theta}_3}\\ &= (m_3 + m_4)l\left\{\ddot{x}(t)\cos\theta_3(t) - \ddot{h}(t)\sin\theta_3(t) + \ddot{l}_1(t)\sin[\theta_3(t)\right.\\ &\quad \left. - \theta_1(t)] - [2\dot{l}_1(t)\dot{\theta}_1(t) + l_1(t)\ddot{\theta}_1(t)]\cos[\theta_3(t) - \theta_1(t)]\right.\\ &\quad \left. - l_1(t)\dot{\theta}_1^2(t)\sin[\theta_3(t) - \theta_1(t)]\right\} + (m_3 + m_4)\\ &\quad \times l^2\left\{\dot{\theta}_2^2(t)\sin[\theta_2(t) - \theta_3(t)] - \ddot{\theta}_2(t)\cos[\theta_2(t) - \theta_3(t)]\right\}\\ &\quad - (m_3 + m_4)l^2\ddot{\theta}_3(t) + m_4 l^2\left\{\dot{\theta}_4^2(t)\sin[\theta_4(t) - \theta_3(t)]\right.\\ &\quad \left. - \ddot{\theta}_4(t)\cos[\theta_4(t) - \theta_3(t)]\right\} \qquad (25)\end{aligned}$$

$$\begin{aligned}F_{\theta_4}^* &= -m_1\boldsymbol{a}_1 \cdot \frac{\partial \boldsymbol{v}_1}{\partial \dot{\theta}_4} - m_2\boldsymbol{a}_2 \cdot \frac{\partial \boldsymbol{v}_2}{\partial \dot{\theta}_4} - m_3\boldsymbol{a}_3 \cdot \frac{\partial \boldsymbol{v}_3}{\partial \dot{\theta}_4} - m_4\boldsymbol{a}_4 \cdot \frac{\partial \boldsymbol{v}_4}{\partial \dot{\theta}_4}\\ &= -m_4\boldsymbol{a}_4 \cdot \frac{\partial \boldsymbol{v}_4}{\partial \dot{\theta}_4}\\ &= m_4 l\{\ddot{x}(t)\cos\theta_4(t) - \ddot{h}(t)\sin\theta_4(t) + \ddot{l}_1(t)\sin[\theta_4(t) - \theta_1(t)]\\ &\quad - [2\dot{l}_1(t)\dot{\theta}_1(t) + l_1(t)\ddot{\theta}_1(t)]\cos[\theta_4(t) - \theta_1(t)]\\ &\quad - l_1(t)\dot{\theta}_1^2(t)\sin[\theta_4(t) - \theta_1(t)]\} + m_4 l^2\left\{\dot{\theta}_2^2(t)\sin[\theta_2(t)\right.\\ &\quad \left. - \theta_4(t)] - \ddot{\theta}_2(t)\cos[\theta_2(t) - \theta_4(t)]\right\} + m_4 l^2\left\{\dot{\theta}_3^2(t)\sin[\theta_3(t)\right.\\ &\quad \left. - \theta_4(t)] - \ddot{\theta}_3(t)\cos[\theta_3(t) - \theta_4(t)]\right\} - m_4 l^2\ddot{\theta}_4(t) \qquad (26)\end{aligned}$$

For n masses, the pattern is as follows:

$$\begin{aligned}F_{\theta_1}^* &= \left(\sum_{j=1}^{n} m_j\right) l_1(\ddot{x}\cos\theta_1 - \ddot{h}\sin\theta_1 - 2\dot{l}_1\dot{\theta}_1 - l_1\ddot{\theta}_1)\\ &\quad + \sum_{i=2}^{n}\left\{\left(\sum_{j=i}^{n} m_j\right) l l_1\left[\dot{\theta}_i^2\sin(\theta_i - \theta_1) - \ddot{\theta}_i\cos(\theta_i - \theta_1)\right]\right\} \qquad (27)\end{aligned}$$

$$\begin{aligned}F_{\theta_k}^* &= \left(\sum_{j=k}^{n} m_j\right) l\left[\ddot{x}\cos\theta_k - \ddot{h}\sin\theta_k + \ddot{l}_1\sin(\theta_k - \theta_1)\right.\\ &\quad \left. - (2\dot{l}_1\dot{\theta}_1 + l_1\ddot{\theta}_1)\cos(\theta_k - \theta_1) - l_1\dot{\theta}_1^2\sin(\theta_k - \theta_1)\right]\\ &\quad + \sum_{i=2}^{n}\left\{\left(\sum_{\substack{j=k\\ j\geq i}}^{n} m_j\right) l^2\left[\dot{\theta}_i^2\sin(\theta_i - \theta_k) - \ddot{\theta}_i\cos(\theta_i - \theta_k)\right]\right\}\\ &\qquad\qquad k = 2, \ldots, n \qquad (28)\end{aligned}$$

Generalized External Forces

If we let the external forces acting on the jth mass be

$$\boldsymbol{F}_j = F_{2(j-1)+1}\boldsymbol{i} + F_{2(j-1)+2}\boldsymbol{j}, \qquad j = 1, \ldots, n \qquad (29)$$

then the generalized forces are as follows:

$$\begin{aligned}F_{\theta_1}^{\text{ext}} &= \boldsymbol{F}_1 \cdot \frac{\partial \boldsymbol{v}_1}{\partial \dot{\theta}_1} + \boldsymbol{F}_2 \cdot \frac{\partial \boldsymbol{v}_2}{\partial \dot{\theta}_1} + \boldsymbol{F}_3 \cdot \frac{\partial \boldsymbol{v}_3}{\partial \dot{\theta}_1} + \boldsymbol{F}_4 \cdot \frac{\partial \boldsymbol{v}_4}{\partial \dot{\theta}_1}\\ &= (\boldsymbol{F}_1 + \boldsymbol{F}_2 + \boldsymbol{F}_3 + \boldsymbol{F}_4) \cdot \frac{\partial \boldsymbol{v}_1}{\partial \dot{\theta}_1}\\ &= -(F_1 + F_3 + F_5 + F_7)l_1(t)\cos\theta_1(t)\\ &\quad + (F_2 + F_4 + F_6 + F_8)l_1(t)\sin\theta_1(t) \qquad (30)\end{aligned}$$

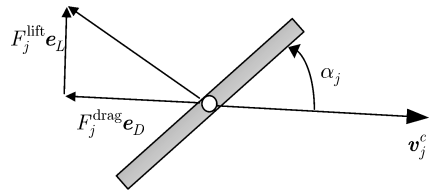

Fig. 2 Orientation of cable segment to the flow.

$$\begin{aligned} F_{\theta_2}^{\text{ext}} &= \boldsymbol{F}_1 \cdot \frac{\partial \boldsymbol{v}_1}{\partial \dot{\theta}_2} + \boldsymbol{F}_2 \cdot \frac{\partial \boldsymbol{v}_2}{\partial \dot{\theta}_2} + \boldsymbol{F}_3 \cdot \frac{\partial \boldsymbol{v}_3}{\partial \dot{\theta}_2} + \boldsymbol{F}_4 \cdot \frac{\partial \boldsymbol{v}_4}{\partial \dot{\theta}_2} \\ &= (\boldsymbol{F}_2 + \boldsymbol{F}_3 + \boldsymbol{F}_4) \cdot \frac{\partial \boldsymbol{v}_2}{\partial \dot{\theta}_2} \\ &= -(F_3 + F_5 + F_7) l \cos\theta_2(t) + (F_4 + F_6 + F_8) l \sin\theta_2(t) \end{aligned} \tag{31}$$

In general, we have

$$F_{\theta_1}^{\text{ext}} = \sum_{j=1}^{n} (-F_{2(j-1)+1} l_1 \cos\theta_1 + F_{2(j-1)+2} l_1 \sin\theta_1) \tag{32}$$

$$F_{\theta_k}^{\text{ext}} = \sum_{j=k}^{n} (-F_{2(j-1)+1} l \cos\theta_k + F_{2(j-1)+2} l \sin\theta_k) \qquad k = 2, \ldots, n \tag{33}$$

Gravity Forces

The gravitational forces are calculated simply from

$$\boldsymbol{F}_j^g = -m_j g \boldsymbol{j} \tag{34}$$

Aerodynamic Forces

For the purposes of calculating the aerodynamic forces acting on the cable, each cable segment is treated as a cylinder. Consider Fig. 2, which shows the orientation of the jth cable segment to the flow. The aerodynamic lift and drag coefficients are defined as functions of the segment angle of attack α_j. The corresponding lift and drag forces are calculated using the velocity of the cable segment relative to the wind. This may be approximated from the motion of the adjacent masses as

$$\boldsymbol{v}_j^c = \left[\left(\boldsymbol{v}_{j-1} - \boldsymbol{v}_{j-1}^{\text{wind}}\right) + \left(\boldsymbol{v}_j - \boldsymbol{v}_j^{\text{wind}}\right)\right]/2 = v_{x_j}^c \boldsymbol{i} + v_{y_j}^c \boldsymbol{j} \tag{35}$$

where $\boldsymbol{v}_j^{\text{wind}}$ is the velocity vector of the wind at the position of the jth mass and the velocity $\boldsymbol{v}_0$ corresponds to the velocity of the aircraft.

The lift and drag coefficients for an inclined circular cylinder are given by[40]

$$C_{D_j} = C_{D_f} + C_{D_{\text{basic}}} \sin^3\alpha_j \approx 0.022 + 1.1 \sin^3\alpha_j \tag{36}$$

$$C_{L_j} = C_{D_{\text{basic}}} \sin^2\alpha_j \cos\alpha_j \approx 1.1 \sin^2\alpha_j \cos\alpha_j \tag{37}$$

We have assumed that the flow around the cable is subcritical. For higher Reynold's numbers, or in the presence of vortex shedding, more complex models of the aerodynamic force coefficients will be required.[41]

The angle of attack may be calculated from

$$\cos\alpha_j = \frac{-\boldsymbol{l}_j \cdot \boldsymbol{v}_j^c}{|\boldsymbol{l}_j|\left|\boldsymbol{v}_j^c\right|} = \frac{v_{x_j}^c \sin\theta_j + v_{y_j}^c \cos\theta_j}{\sqrt{\left(v_{x_j}^c\right)^2 + \left(v_{y_j}^c\right)^2}} \tag{38}$$

where

$$\boldsymbol{l}_j = -l_j \sin\theta_j \boldsymbol{i} - l_j \cos\theta_j \boldsymbol{j} \tag{39}$$

The unit vectors defining the directions of the lift and drag vectors are

$$\boldsymbol{e}_D = -\frac{\boldsymbol{v}_j^c}{\left|\boldsymbol{v}_j^c\right|} \tag{40}$$

$$\boldsymbol{e}_L = -\frac{\left(\boldsymbol{v}_j^c \times \boldsymbol{l}_j\right) \times \boldsymbol{v}_j^c}{\left|\left(\boldsymbol{v}_j^c \times \boldsymbol{l}_j\right) \times \boldsymbol{v}_j^c\right|} = \frac{\boldsymbol{k} \times \boldsymbol{v}_j^c}{\left|\boldsymbol{v}_j^c\right|} \tag{41}$$

where $\boldsymbol{k}$ is a unit vector normal to the plane of motion.

Hence, the lift and drag vectors may be written as

$$\boldsymbol{F}_j^{\text{drag}} = \tfrac{1}{2}\rho C_{D_j} l_j d \left|\boldsymbol{v}_j^c\right|^2 \boldsymbol{e}_D = -\tfrac{1}{2}\rho C_{D_j} l_j d \left|\boldsymbol{v}_j^c\right| \left[v_{x_j}^c \boldsymbol{i} + v_{y_j}^c \boldsymbol{j}\right] \tag{42}$$

$$\boldsymbol{F}_j^{\text{lift}} = \tfrac{1}{2}\rho C_{L_j} l_j d \left|\boldsymbol{v}_j^c\right|^2 \boldsymbol{e}_L = \tfrac{1}{2}\rho C_{L_j} l_j d \left|\boldsymbol{v}_j^c\right| \left[-v_{y_j}^c \boldsymbol{i} + v_{x_j}^c \boldsymbol{j}\right] \tag{43}$$

These lift and drag vectors are assumed to be constant over each cable segment. Hence, the aerodynamic forces are lumped to each point mass taking half from each adjacent segment,

$$\boldsymbol{F}_j^{\text{aero}} = \left(\boldsymbol{F}_{j-1}^{\text{drag}} + \boldsymbol{F}_j^{\text{drag}}\right)/2 + \left(\boldsymbol{F}_{j-1}^{\text{lift}} + \boldsymbol{F}_j^{\text{lift}}\right)/2 \tag{44}$$

The towed vehicle is assumed to be spherical, generating drag only.

Kane's Equations

Application of Kane's equations yields the equations of motion ($n = 4$),

$$\begin{aligned} &(m_1 + m_2 + m_3 + m_4) l_1(t) [\ddot{x}(t)\cos\theta_1(t) - \ddot{h}(t)\sin\theta_1(t) \\ &\quad - 2\dot{l}_1(t)\dot{\theta}_1(t) - l_1(t)\ddot{\theta}_1(t)] + (m_2 + m_3 + m_4) \\ &\quad \times l l_1(t)\left\{\dot{\theta}_2^2(t)\sin[\theta_2(t) - \theta_1(t)] - \ddot{\theta}_2(t)\cos[\theta_2(t) - \theta_1(t)]\right\} \\ &\quad + (m_3 + m_4) l l_1(t)\left\{\dot{\theta}_3^2(t)\sin[\theta_3(t) - \theta_1(t)] - \ddot{\theta}_3(t)\cos[\theta_3(t) \right. \\ &\quad \left. - \theta_1(t)]\right\} + m_4 l l_1(t)\left\{\dot{\theta}_4^2(t)\sin[\theta_4(t) - \theta_1(t)] \right. \\ &\quad \left. - \ddot{\theta}_4(t)\cos[\theta_4(t) - \theta_1(t)]\right\} - (F_1 + F_3 + F_5 + F_7) l_1(t)\cos\theta_1(t) \\ &\quad + (F_2 + F_4 + F_6 + F_8) l_1(t)\sin\theta_1(t) = 0 \end{aligned} \tag{45}$$

$$\begin{aligned} &(m_2 + m_3 + m_4) l \left\{\ddot{x}(t)\cos\theta_2(t) - \ddot{h}(t)\sin\theta_2(t) + \ddot{l}_1(t)\sin[\theta_2(t) \right. \\ &\quad - \theta_1(t)] - [2\dot{l}_1(t)\dot{\theta}_1(t) + l_1(t)\ddot{\theta}_1(t)]\cos[\theta_2(t) - \theta_1(t)] \\ &\quad \left. - l_1(t)\dot{\theta}_1^2(t)\sin[\theta_2(t) - \theta_1(t)]\right\} - (m_2 + m_3 + m_4) l^2 \ddot{\theta}_2(t) \\ &\quad + (m_3 + m_4) l^2 \left\{\dot{\theta}_3^2(t)\sin[\theta_3(t) - \theta_2(t)] - \ddot{\theta}_3(t)\cos[\theta_3(t) \right. \\ &\quad \left. - \theta_2(t)]\right\} + m_4 l^2 \left\{\dot{\theta}_4^2(t)\sin[\theta_4(t) - \theta_2(t)] - \ddot{\theta}_4(t)\cos[\theta_4(t) \right. \\ &\quad \left. - \theta_2(t)]\right\} - (F_3 + F_5 + F_7) l \cos\theta_2(t) \\ &\quad + (F_4 + F_6 + F_8) l \sin\theta_2(t) = 0 \end{aligned} \tag{46}$$

$$\begin{aligned} &(m_3 + m_4) l \left\{\ddot{x}(t)\cos\theta_3(t) - \ddot{h}(t)\sin\theta_3(t) + \ddot{l}_1(t)\sin[\theta_3(t) \right. \\ &\quad - \theta_1(t)] - [2\dot{l}_1(t)\dot{\theta}_1(t) + l_1(t)\ddot{\theta}_1(t)]\cos[\theta_3(t) - \theta_1(t)] \\ &\quad \left. - l_1(t)\dot{\theta}_1^2(t)\sin[\theta_3(t) - \theta_1(t)]\right\} + (m_3 + m_4) \\ &\quad \times l^2 \left\{\dot{\theta}_2^2(t)\sin[\theta_2(t) - \theta_3(t)] - \ddot{\theta}_2(t)\cos[\theta_2(t) - \theta_3(t)]\right\} \\ &\quad - (m_3 + m_4) l^2 \ddot{\theta}_3(t) + m_4 l^2 \left\{\dot{\theta}_4^2(t)\sin[\theta_4(t) - \theta_3(t)] \right. \\ &\quad \left. - \ddot{\theta}_4(t)\cos[\theta_4(t) - \theta_3(t)]\right\} - (F_5 + F_7) l \cos\theta_3(t) \\ &\quad + (F_6 + F_8) l \sin\theta_3(t) = 0 \end{aligned} \tag{47}$$

$$\begin{aligned} &m_4 l \left\{\ddot{x}(t)\cos\theta_4(t) - \ddot{h}(t)\sin\theta_4(t) + \ddot{l}_1(t)\sin[\theta_4(t) - \theta_1(t)] \right. \\ &\quad - [2\dot{l}_1(t)\dot{\theta}_1(t) + l_1(t)\ddot{\theta}_1(t)]\cos[\theta_4(t) - \theta_1(t)] \\ &\quad \left. - l_1(t)\dot{\theta}_1^2(t)\sin[\theta_4(t) - \theta_1(t)]\right\} + m_4 l^2 \left\{\dot{\theta}_2^2(t)\sin[\theta_2(t) \right. \\ &\quad \left. - \theta_4(t)] - \ddot{\theta}_2(t)\cos[\theta_2(t) - \theta_4(t)]\right\} + m_4 l^2 \left\{\dot{\theta}_3^2(t)\sin[\theta_3(t) \right. \\ &\quad \left. - \theta_4(t)] - \ddot{\theta}_3(t)\cos[\theta_3(t) - \theta_4(t)]\right\} - m_4 l^2 \ddot{\theta}_4(t) \\ &\quad - F_7 l \cos\theta_4(t) + F_8 l \sin\theta_4(t) = 0 \end{aligned} \tag{48}$$

In matrix form, these coupled equations become

$$\boldsymbol{M}\ddot{\boldsymbol{q}} = \boldsymbol{B} \tag{49}$$

where

$$\boldsymbol{M} = \begin{bmatrix} (m_1+m_2+m_3+m_4)l_1^2 & (m_2+m_3+m_4)ll_1\cos(\theta_2-\theta_1) & (m_3+m_4)ll_1\cos(\theta_3-\theta_1) & m_4ll_1\cos(\theta_4-\theta_1) \\ (m_2+m_3+m_4)ll_1\cos(\theta_2-\theta_1) & (m_2+m_3+m_4)l^2 & (m_3+m_4)l^2\cos(\theta_3-\theta_2) & m_4l^2\cos(\theta_4-\theta_2) \\ (m_3+m_4)ll_1\cos(\theta_3-\theta_1) & (m_3+m_4)l^2\cos(\theta_3-\theta_2) & (m_3+m_4)l^2 & m_4l^2\cos(\theta_4-\theta_3) \\ m_4ll_1\cos(\theta_4-\theta_1) & m_4l^2\cos(\theta_4-\theta_2) & m_4l^2\cos(\theta_4-\theta_3) & m_4l^2 \end{bmatrix} \tag{50}$$

$$\begin{aligned} B_1 &= (m_1+m_2+m_3+m_4)l_1(\ddot{x}\cos\theta_1 - \ddot{h}\sin\theta_1 - 2\dot{l}_1\dot{\theta}_1) \\ &\quad + (m_2+m_3+m_4)ll_1\dot{\theta}_2^2\sin(\theta_2-\theta_1) \\ &\quad + (m_3+m_4)ll_1\dot{\theta}_3^2\sin(\theta_3-\theta_1) + m_4ll_1\dot{\theta}_4^2\sin(\theta_4-\theta_1) \\ &\quad - (F_1+F_3+F_5+F_7)l_1\cos\theta_1 \\ &\quad + (F_2+F_4+F_6+F_8)l_1\sin\theta_1 \end{aligned} \tag{51}$$

$$\begin{aligned} B_2 &= (m_2+m_3+m_4)l\big[\ddot{x}\cos\theta_2 - \ddot{h}\sin\theta_2 + \ddot{l}_1\sin(\theta_2-\theta_1) \\ &\quad - 2\dot{l}_1\dot{\theta}_1\cos(\theta_2-\theta_1) - l_1\dot{\theta}_1^2\sin(\theta_2-\theta_1)\big] \\ &\quad + (m_3+m_4)l^2\dot{\theta}_3^2\sin(\theta_3-\theta_2) + m_4l^2\dot{\theta}_4^2\sin(\theta_4-\theta_2) \\ &\quad - (F_3+F_5+F_7)l\cos\theta_2 + (F_4+F_6+F_8)l\sin\theta_2 \end{aligned} \tag{52}$$

$$\begin{aligned} B_3 &= (m_3+m_4)l\big[\ddot{x}\cos\theta_3 - \ddot{h}\sin\theta_3 + \ddot{l}_1\sin(\theta_3-\theta_1) \\ &\quad - 2\dot{l}_1\dot{\theta}_1\cos(\theta_3-\theta_1) - l_1\dot{\theta}_1^2\sin(\theta_3-\theta_1)\big] \\ &\quad + (m_3+m_4)l^2\dot{\theta}_2^2\sin(\theta_2-\theta_3) + m_4l^2\dot{\theta}_4^2\sin(\theta_4-\theta_3) \\ &\quad - (F_5+F_7)l\cos\theta_3 + (F_6+F_8)l\sin\theta_3 \end{aligned} \tag{53}$$

$$\begin{aligned} B_4 &= m_4l\big[\ddot{x}\cos\theta_4 - \ddot{h}\sin\theta_4 + \ddot{l}_1\sin(\theta_4-\theta_1) \\ &\quad - 2\dot{l}_1\dot{\theta}_1\cos(\theta_4-\theta_1) - l_1\dot{\theta}_1^2\sin(\theta_4-\theta_1)\big] + m_4l^2\dot{\theta}_2^2\sin(\theta_2-\theta_4) \\ &\quad + m_4l^2\dot{\theta}_3^2\sin(\theta_3-\theta_4) - F_7l\cos\theta_4 + F_8l\sin\theta_4 \end{aligned} \tag{54}$$

and $\ddot{\boldsymbol{q}} = [\ddot{\theta}_1, \ldots, \ddot{\theta}_n]^T$.

In the general case, the symmetrical mass matrix $\boldsymbol{M}$ has its upper triangular entries defined by

$$M_{ki} := \begin{cases} \displaystyle\sum_{j=1}^{n} m_j l_1^2, & k=1, i=1 \\ \displaystyle\sum_{j=i}^{n} m_j l l_1\cos(\theta_i-\theta_1), & k=1, i\neq 1 \\ \displaystyle\sum_{j=k}^{n} m_j l^2, & k=i, k\neq 1 \\ \displaystyle\sum_{j=i}^{n} m_j l^2\cos(\theta_i-\theta_k), & k\neq i, k\neq 1 \end{cases} \tag{55}$$

The entries of the $\boldsymbol{B}$ vector are obtained as

$$\begin{aligned} B_1 &= \left[\sum_{j=1}^{n} m_j\right] l_1(\ddot{x}\cos\theta_1 - \ddot{h}\sin\theta_1 - 2\dot{l}_1\dot{\theta}_1) \\ &\quad + \sum_{i=2}^{n}\left[\left(\sum_{j=i}^{n} m_j\right) l l_1\dot{\theta}_i^2\sin(\theta_i-\theta_1)\right] \\ &\quad + \sum_{j=1}^{n}(-F_{2(j-1)+1}l_1\cos\theta_1 + F_{2(j-1)+2}l_1\sin\theta_1) \end{aligned}$$

$$\begin{aligned} B_k &= \left[\sum_{j=k}^{n} m_j\right] l\big[\ddot{x}\cos\theta_k - \ddot{h}\sin\theta_k + \ddot{l}_1\sin(\theta_k-\theta_1) \\ &\quad - 2\dot{l}_1\dot{\theta}_1\cos(\theta_k-\theta_1) - l_1\dot{\theta}_1^2\sin(\theta_k-\theta_1)\big] \\ &\quad + \sum_{i=2}^{n}\left[\left(\sum_{\substack{j=k \\ j\geq i}}^{n} m_j\right) l^2\dot{\theta}_i^2\sin(\theta_i-\theta_k)\right] \\ &\quad + \sum_{j=k}^{n}(-F_{2(j-1)+1}l\cos\theta_k + F_{2(j-1)+2}l\sin\theta_k) \end{aligned}$$

$$k = 2, \ldots, n \tag{56}$$

The equations of motion may be cast in state-space form as

$$\dot{\boldsymbol{x}}(t) = \begin{bmatrix} \dot{\boldsymbol{q}}(t) \\ \ddot{\boldsymbol{q}}(t) \end{bmatrix} \tag{57}$$

Guidance for Payload Pickup

In this section, a guidance approach for maneuvering the towed body by cable reeling is developed. There have been related studies on the use of tether reeling to control the motion of the tether tip. For example, Lorenzini et al.[42] developed the nonlinear optimal open-loop control law for Small Expendable Deployment System-II (SEDS-II) by a direct shooting method that optimized the number of brake turns on the SEDS barberpolelike deployer. The goal of the approach in Ref. 42 was to minimize the residual rigid-body motions of the tether following deployment to the local vertical. The optimization problem was solved using a simplex direct search method. One key difference between the control of tethered satellite systems by tether reeling and an aircraft-towed system close to the Earth is that the control forces on a tethered satellite are generated by Coriolis forces caused by the orbital motion. In contrast, control of an aerial-towed-cable system is achieved by controlling the deployed cable length, which alters the amount of drag on the system and, hence, the cable's angular rotation.

The general guidance problem considered in this paper is to maneuver the tip of the cable from a given initial state to rendezvous with a known target while avoiding collision with any terrain. For single rendezvous opportunities, the guidance problem is a relatively straightforward matter of deploying the cable to the correct altitude. However, how the cable should be deployed, that is, time-optimal deployment or otherwise, is still a design variable. For more complex scenarios, such as that studied in this section, the cable must be deployed and retrieved to hit multiple targets while avoiding any terrain. Therefore, the guidance problem is much more complex. To give a unique trajectory with smooth reel dynamics, the guidance problem is solved to minimize the reel acceleration $\ddot{l}_1$. In this study, the aircraft motion is assumed to be fixed, and hence, minimizing the reel acceleration is a good measure of penalizing the overall control performance of the system. In terms of practical implementation, we assume that global positioning system coordinates of the towed body and aircraft would be available. It may also be necessary to estimate the cable curvature by measuring the slope and tension of the cable at the attachment points. Other methods for sensing the cable shape are currently being investigated.[2,3]

Optimal Control Problem

The optimal control problem may be posed as follows. Determine the control input $\ddot{l}_1(t)$ and corresponding state trajectory $\boldsymbol{x}(t) = [\boldsymbol{q}(t), \dot{\boldsymbol{q}}(t)]$ to minimize the performance index

$$\mathcal{J} = \int_0^{t_f} \ddot{l}_1^2\,\mathrm{d}t \tag{58}$$

subject to the state equations (57), the boundary conditions,

$$\psi_0(\boldsymbol{x}_0, t_0) = \mathbf{0} \tag{59}$$

$$\psi_f(\boldsymbol{x}_f, t_f) = \mathbf{0} \tag{60}$$

the event conditions,

$$\psi_e(\boldsymbol{x}_e, t_e) = \mathbf{0} \tag{61}$$

and the path constraints,

$$\boldsymbol{g}(\boldsymbol{x}(t), t) \leq \mathbf{0} \tag{62}$$

In this setting, the final time t_f and the event time t_e are free.

Boundary and Event Conditions

The initial conditions are selected to be the cable's equilibrium position for the given aircraft speed and deployed cable parameters. The equilibrium position is determined by solving the equations of motion such that the angular accelerations and angular velocities of each link are zero. This has been implemented using a nonlinear root-finding algorithm in MATLAB®. Alternatively, one may integrate the equations of motion for a sufficiently long period to allow any residual oscillations to damp out. For the simulation parameters used in this paper, it takes only a few minutes for the cable to reach relative equilibrium. Either way, the resulting set of initial conditions define the boundary conditions at the initial time.

The event conditions and the final boundary conditions are formulated in identical ways. The desired position of the cable tip is prescribed in the inertial coordinate system by the constraints

$$x_{\text{aircraft}}(t_k) - \sum_{j=1}^{n} l_j(t_k) \sin\theta_j(t_k) = x_{\text{target}}(t_k), \qquad k \in [e, f] \tag{63}$$

$$h_{\text{aircraft}}(t_k) - \sum_{j=1}^{n} l_j(t_k) \cos\theta_j(t_k) = h_{\text{target}}(t_k), \qquad k \in [e, f] \tag{64}$$

where the coordinates x_{target} and h_{target} are the known coordinates of the ground targets. Note that these have different values depending on the event e and final boundary targets f. At the instant of rendezvous, the cable length rate must be zero, and so we have

$$\dot{l}_1(t_k) = 0, \qquad k \in [e, f] \tag{65}$$

Path Constraints

The path constraint in this problem arises from the need to avoid collisions between the towed vehicle and the ground or local elevated terrain. The constraint is dependent on both the x and y position of the towed vehicle, as well as the shape of the terrain. In general, we must have

$$h_{\text{terrain}}\left[x_{\text{aircraft}}(t) - \sum_{j=1}^{n} l_j(t) \sin\theta_j(t)\right] + y_{\text{tol}} \leq h_{\text{aircraft}}(t) - \sum_{j=1}^{n} l_j(t) \cos\theta_j(t) \tag{66}$$

where y_{tol} is the safety tolerance to avoid any contact with the terrain, set to be 1 m in this work. Note that this constraint depends on all angular rotations of the links.

Numerical Solution Method

The optimal control problem described in the preceding section is solved using direct transcription methods. A general purpose software package implemented in MATLAB and utilizing the solver SNOPT[43] is employed. The original version of the software, called DIRECT,[44] handles only single-phase optimal control problems but implements a wide range of discretization techniques. A newer version of this software for multiple-phase problems has been developed. Although a range of discretization methods are available, such as pseudospectral methods[45,46] and Runge–Kutta methods (see Ref. 47), the Hermite–Simpson method (see Ref. 48) has been used in this paper because it was found to converge more readily for the guesses and situations provided. Constraint Jacobians of the resulting nonlinear programming problem are estimated using sparse finite differences. In all cases, the initial guess was provided as the cable equilibrium position with zero control input.

Numerical Case Study

To study the features of the optimal cable dynamics during payload pickup, a standard scenario has been selected. In this scenario, two pickup maneuvers separated by an elevated piece of terrain are to occur. The aircraft is initially positioned at $x = 0$, and the cable is initially in equilibrium with a deployed length of 600 m. The initial configuration is such that the cable tip is roughly 405.60 m from the first target with an altitude error of 122.29 m. The key system parameters are listed in Table 1. At the instant of the first pickup, a mass of 50 kg is added to the end of the cable.

In this example case, there is assumed to be terrain between the first and second targets so that two clear snatches are not possible. For simplicity, the terrain is modeled as a simple sine wave according to

$$y_{\text{terrain}} = \begin{cases} h_t \sin(\pi[x - 500]/400), & 500 \leq x \leq 900 \\ 0, & \text{otherwise} \end{cases} \tag{67}$$

The number of point masses representing the cable is taken to be 6 for the numerical computations in this section. Initially all cable elements have the same length of 100 m, including the first element.

Effect of Terrain Height

A sequence of problems was solved by varying the terrain height from 0 to 110 m in increments of 10 m to examine the effect of the terrain avoidance maneuver on the optimal reeling dynamics. In general, increasing the height of the terrain causes an increase in the cost function, as shown in Fig. 3, indicating that more active control is required as the terrain height increases. In fact, Fig. 3 illustrates a nearly quadratic increase in cost as the terrain height increases. This effect can be clearly seen in Fig. 4, which shows the control input for each optimal trajectory. There are several points to note from Fig. 4. First, there is a noticeable discontinuity in the controls at the instant of the first pickup. The reel acceleration changes suddenly because the first pickup requires the cable length rate to be zero, but during the second phase the terrain must be avoided by retrieving some of the cable. Therefore, the controls do not remain continuous. The second point to note is that increasing the height of the terrain has a noticeable effect on the controls in the second phase, regardless of the terrain height. This is expected because the second phase contains the terrain that must be avoided. However, as the height of the terrain increases, the control in the first phase also

Table 1 Multiple air-cable pickup parameters

Property	Value
Initial end mass m_{end}	100 kg
Cable diameter d	2 mm
Projected area of towed vehicle A_{end}	0.5 m^2
Drag coefficient of towed vehicle $C_{D_{\text{end}}}$	0.5
Altitude of aircraft	550 m
Aircraft speed	45 m/s
Initial cable length	600 m
Cable density	7850 kg/m^3
Air density	1.225 kg/m^3
Number of cable elements n	6
Length of each cable element[a] l	100 m
First pickup	
x_{target}	400 m
h_{target}	2 m
Second pickup	
x_{target}	1000 m
h_{target}	2 m

[a]Also denotes the initial length of the first cable segment $l_1(0)$.

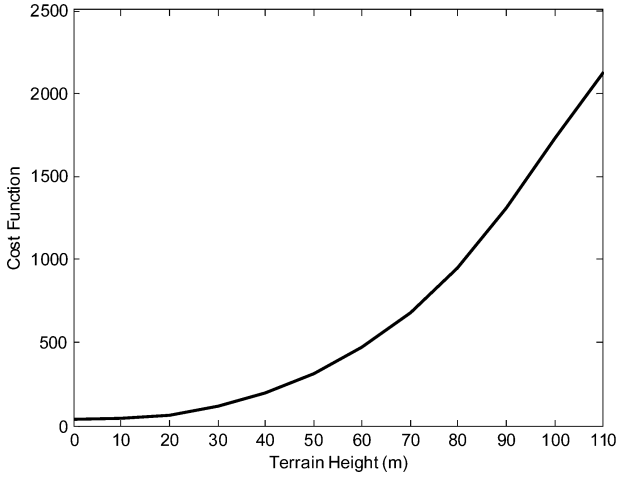

Fig. 3 Effect of terrain height on cost function value.

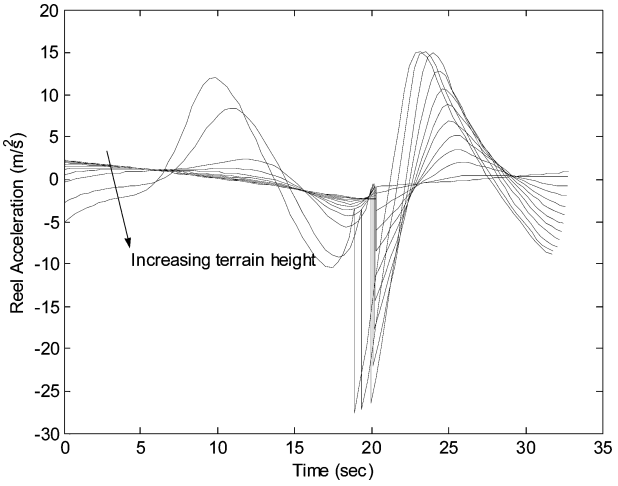

Fig. 4 Control input for increasing terrain height.

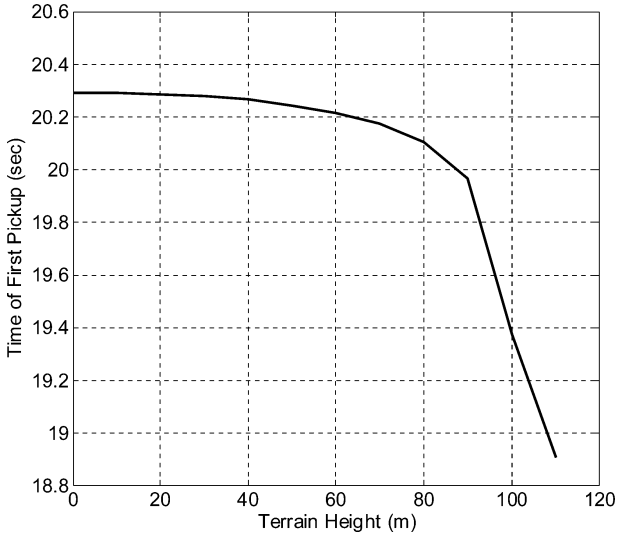

Fig. 5 Effect of terrain height on time of first pickup.

begins to change. In concert with this is a downward shift in the time of the first pickup, as shown in Fig. 5. It appears that as the height of the terrain increases, it becomes necessary to influence the cable dynamics in the first phase so that the cable tip reaches its first target sooner than would be necessary when there are no terrain changes. Because the aircraft speed is fixed, this then allows additional time to meet the objectives of the second phase. In particular, it allows for the additional time needed to avoid colliding with the terrain.

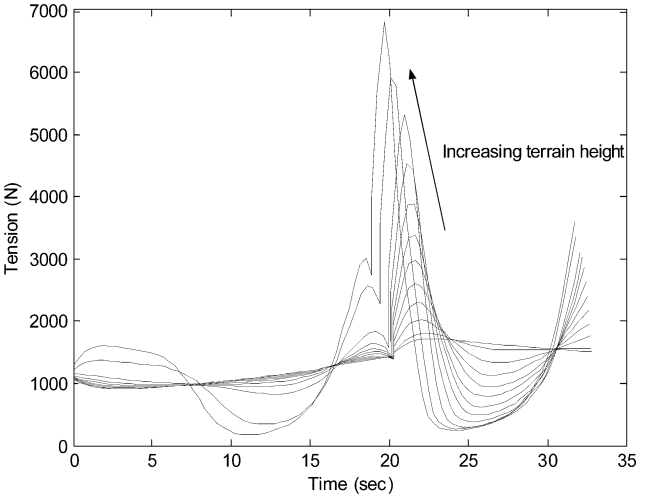

Fig. 6 Cable tension at aircraft during multiple pickup maneuver for increasing terrain height.

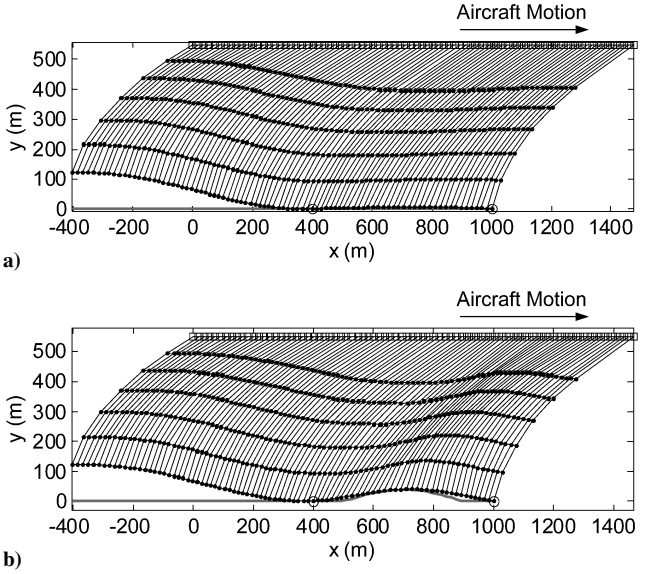

Fig. 7 Cable orientation during multiple pickup scenario with a) no elevated terrain and b) 40-m elevated terrain.

Figure 6 shows the cable tension at the aircraft end, calculated from the optimal trajectories. The tension exhibits a discontinuity at the first payload pickup point. This is due to the combination of sudden change in the reel acceleration, as well as the increased mass at the end of the cable after picking up the first payload. It becomes evident from Fig. 6 that the reel accelerations required for the high-terrain cases cause significant peaks in the cable tension. It can also be seen that large positive reel accelerations could potentially result in a slack (zero tension) cable. This might be dangerous if the cable transitions between slack and taut states because of possible longitudinal and/or transverse traveling waves that might adversely affect the motion of the towed vehicle.

Figures 7 and 8 show the effect of increasing terrain height on the cable dynamics during the maneuver. Figure 7a shows the case for $h_t = 0$, Fig. 7b shows the case for $h_t = 40$ m, and Figs. 8a and 8b show the cases for $h_t = 70$ and 110 m, respectively. Figures 7a and 7b shows that the small amount of cable reeling needed for low terrain does not greatly influence the cable orientation and shape. However, Figs. 8a and 8b show that lateral oscillations are initiated by the rapid reeling required to safely clear the terrain. This effect is even more pronounced in Fig. 8b, which shows some rather large lateral motion of the cable. It appears that these lateral dynamics are necessary to allow the cable tip to reach its target sooner than would otherwise be possible. This is achieved by the geometric shortening

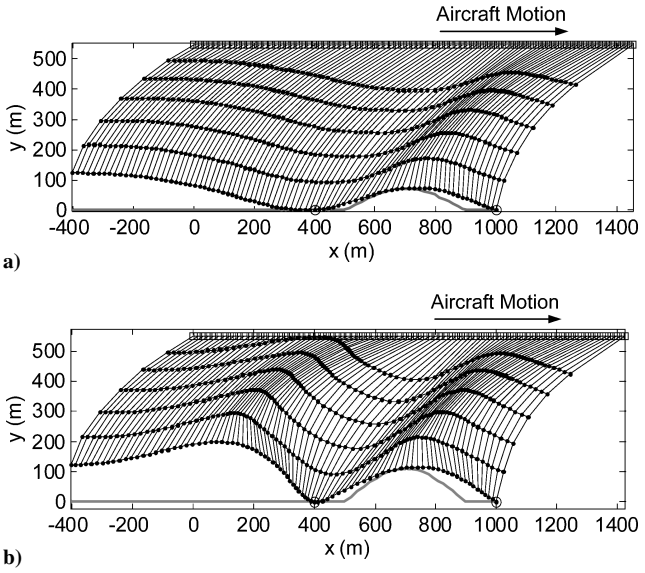

Fig. 8 Cable orientation during multiple pickup scenario with a) 70-m elevated terrain and b) 110-m elevated terrain.

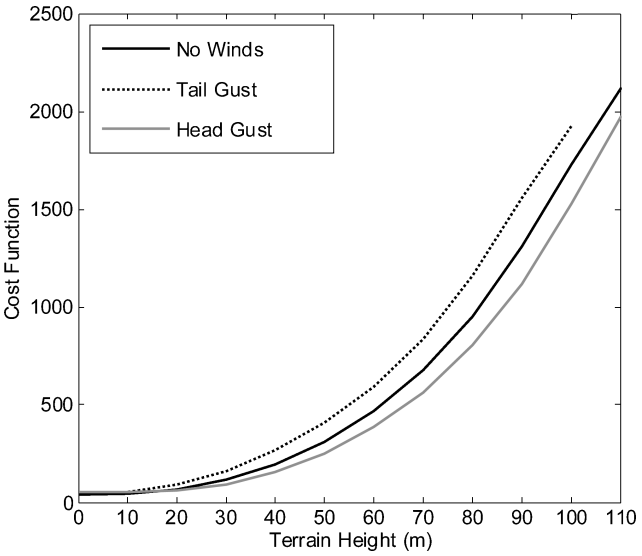

Fig. 9 Cost function value for increasing terrain height with head and tail gusts.

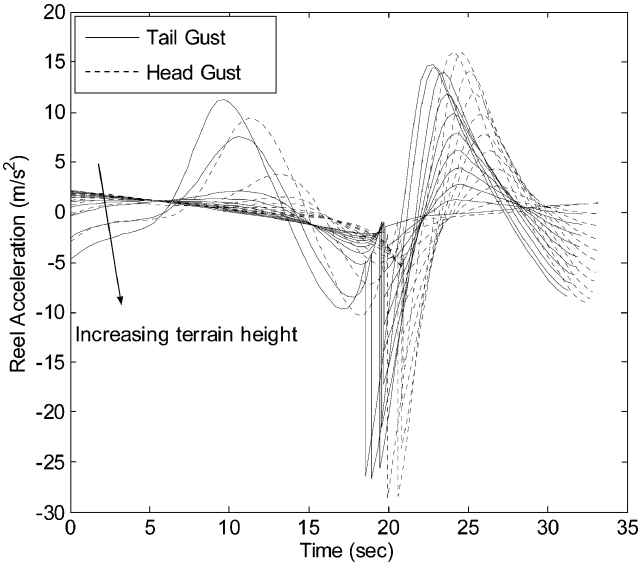

Fig. 10 Control input for increasing terrain height and wind gusts.

or lengthening of the tip displacement by the transverse motion of the cable. The lateral deflections of the point masses representing the cable were calculated by defining a line from the towpoint to the position of the towed vehicle. The maximum deflection of the cable in the case of no elevated terrain is approximately 73 m, whereas for 50-m elevated terrain the deflection increases to approximately 88.5 m, and for 110-m elevated terrain the deflection is approximately 132.4 m. It is clear that there is a complex interaction between the reel dynamics, the amount of cable deployed, and the resulting optimal trajectories for the system. It is also evident that for this particular study separating the two phases into distinct optimal control problems results in suboptimal performance. These results demonstrate that there is a tight coupling between phases that is strongly dependent on the height of the terrain in the second phase.

Effect of Gust

In the preceding section, the atmosphere was assumed to be motionless with respect to the ground. To assess the effect of wind gusts on the optimal dynamics, a simple horizontal wind gust was modeled using a half sine-wave as follows:

$$v_x^{\text{wind}} = \begin{cases} \pm 10 \sin(\pi[x - 200]/200), & 200 \le x \le 400 \\ 0, & \text{otherwise} \end{cases} \tag{68}$$

The identical sequence of optimal control problems was solved with the effect of the wind disturbance included, for both tail gusts and head gusts. The results are qualitatively similar to the case with no wind, except that the cost function values are approximately 10–20% lower (head gusts) or higher (tail gusts) than the no wind cases, as shown in Fig. 9. It can be seen from Fig. 9 that a head gust actually aids the system dynamics, whereas a tail gust degrades the performance. Also note that in the case of a tail gust with 110-m-high terrain, the optimizer failed to find a solution. This is likely due to the length of the first link in the model becoming negative in length, rather than the maneuver not being possible. These results can be inferred from Fig. 10, which shows the control inputs for both tail and head gust cases. This should be compared with Fig. 4, particularly during the first phase near the first pickup point. It is evident that the direction of the gust has a strong influence on the optimal maneuver, although the qualitative nature of the maneuver remains unchanged. It can also be seen that this maneuver is easier to perform when the aircraft is flying into a head wind, as can be inferred from the negative gust results. A head gust causes the cable to lag farther behind the aircraft near the first pickup point. This allows more time to avoid the terrain safely in the second phase.

Effect of Wind Strength

In the preceding section, the effect of a short gust in combination with an increase in terrain height was examined. In this section, the effect of different strength winds for the case of no elevated terrain is considered. In this study, the wind profile is taken to be

$$v_x^{\text{wind}} = \begin{cases} v_w \sin(\pi x/800), & 0 \le x \le 800 \\ 0, & \text{otherwise} \end{cases} \tag{69}$$

where v_w is varied from -19 to $+19$ m/s. A summary of the results of the optimum cost function is shown in Fig. 11. This summary shows that in the absence of terrain, small tail winds can improve the maneuver slightly, whereas larger tail wind velocities result in a net increase in the cost function compared to the case with no wind. The control input time history for the head wind cases are shown in Fig. 12a, and the tail wind cases are shown in Fig. 12b. It is evident from Fig. 12 that there is indeed a strong dependency of the controls on the direction and magnitude of the winds. In the negative wind cases, the control effort is almost exclusively in the first phase, with only small corrections in the second phase of the maneuver. In conjunction with this is an increase in the maneuver time by approximately 5 s. This is due to the increase in drag on

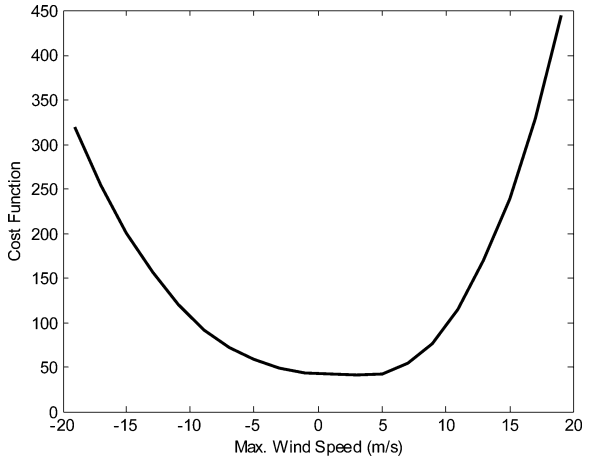

Fig. 11 Cost function value for varying maximum wind speed.

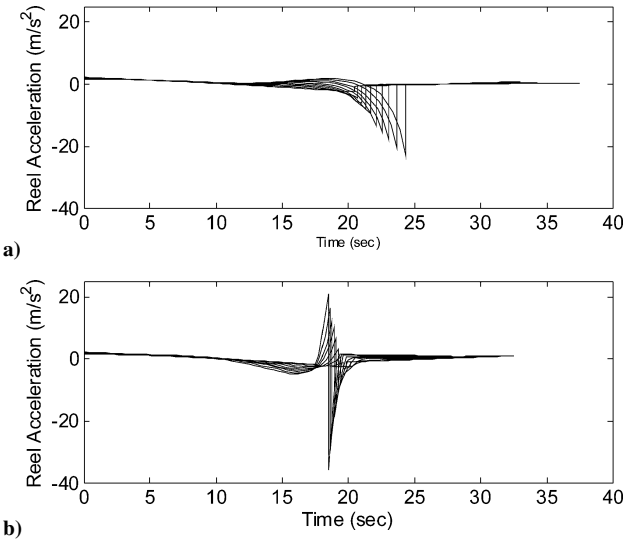

Fig. 12 Control input a) for head winds and b) for tail winds.

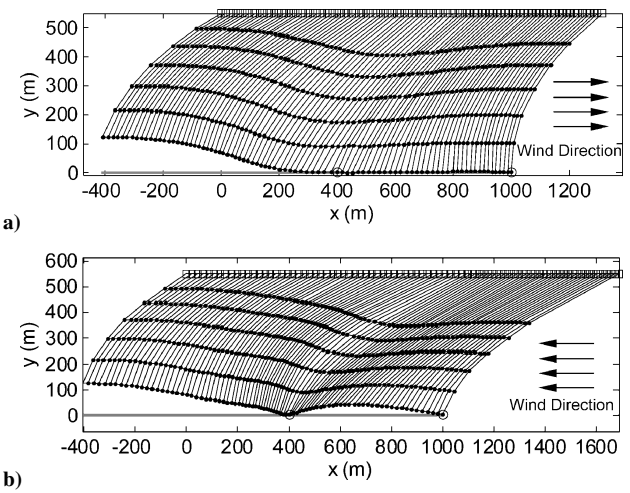

Fig. 13 Cable orientation during multiple pickup scenario with a) 19-m/s maximum tail wind and b) 19 m/s maximum head wind.

the system, which causes the cable system to lag farther behind the aircraft when compared with the case of no wind. For the case of a tail wind, some significant reeling must occur in both phases, as shown in Fig. 12b. The cable shape for the 19-m/s tail wind case is shown in Fig. 13a, and the 19 m/s head wind case is shown in Fig. 13b. A comparison of Fig. 13a with Fig. 13b reveals the significant lag of the towed vehicle with respect to the aircraft for the case of a head wind. Figure 13b also shows a natural altitude increase in the towed vehicle after the first pickup that would aid in avoiding any terrain between the first and second pickups and explains why the head wind proved beneficial in the preceding section (Figs. 9 and 10).

Conclusions

Optimal control of an aerial-towed-cable system for multiple payload pickups has been studied for the case of a flexible, variable length cable. The cable can be efficiently modeled using a lumped parameter method, which connects a series of point masses via rigid-link elements. When the length of deployed cable is controlled via the winch reel acceleration, it is possible to maneuver the towed vehicle to hit multiple ground targets with precision. In an example scenario, the effect of terrain between two targets requires special attention by the control system. As the height of the terrain increases, the control action required also increases. It becomes necessary to affect large changes in the reel acceleration to alter the cable lateral dynamics and swinging motion so that the tip of the cable can hit its targets and safely avoid collision with the terrain. The effect of wind gusts on the optimal dynamics were also shown to be dependent on the direction of the wind. A head wind in conjunction with increasing terrain height was found to aid the maneuver, whereas a tail wind requires more work from the controller. This is due to the tendency of the payload to increase in altitude after the first pickup, as was observed for the case with no terrain and various wind speeds.

References

[1]Trivailo, P., Blanksby, C., Sgarioto, D., Williams, P., and Smart, R., "Defence Applications for Cable Systems Deployed from Aerial and Naval Platforms," *Proceedings of the Land Warfare Conference*, edited by V. Puri, D. Filippidis, S. Quinn, and J. Kelly, Defense Science and Technology Office, Edinburgh, South Australia, 2003, pp. 285–294.

[2]Wright, G., Knox, B., Drack, L., Wharington, J., Jackson, P., Trivailo, P., Blanksby, C., and Williams, P., "Dynamics of UUV Umbilical Cables—Computer Simulation and Experimental Measurements," *Pacific 2002 International Maritime Conference*, Inst. of Marine Engineers, Paper IMC-Navi-10.1, Kambah, Australia, Jan. 2002.

[3]Wright, G., Knox, B., Drack, L., Wharington, J., Jackson, P., Trivailo, P., Blanksby, C., and Williams, P., "Improving ROV Tether Management Through Dynamic Cable Prediction Modelling and Visualization," *Undersea Defence Technology*, Nexus Media Communications, Paper 87, Kent, United Kingdom, Oct. 2002.

[4]Quisenberry, J. E., and Arena, A. S., "Dynamic Simulation of Low Altitude Aerial Tow System," AIAA Paper 2004-4813, Aug. 2004.

[5]Williams, P., and Trivailo, P., "Cable Deployment Control for Towed Aerial-Cable Payload Pick-Up and Delivery System," *Proceedings of the Land Warfare Conference*, edited by V. Puri, D. Filippidis, P. Retter, and J. Kelly, Defense Science and Technology Office, Edinburgh, South Australia, 2004, pp. 313–329.

[6]Skop, R. A., and Choo, Y.-I., "The Configuration of a Cable Towed in a Circular Path," *Journal of Aircraft*, Vol. 8, No. 11, 1971, pp. 856–862.

[7]Clifton, J. M., Schmidt, L. V., and Stuart, T. D., "Dynamic Modeling of a Trailing Wire Towed by an Orbiting Aircraft," *Journal of Guidance, Control, and Dynamics*, Vol. 18, No. 4, 1995, pp. 875–881.

[8]O'Donnell, J., "Air Pick-Up," *EnRoute*, Vol. 9, No. 1, 2000, URL: http://www.postalmuseum.si.edu/resources/6a2w_airpickup.html [cited 29 Nov. 2005].

[9]Purvis, P., "Fulton's Skyhook: An Early Method of Crew Extraction," *Flight Journal*, Sept./Oct. 2004, URL: http://www.flightjournal.com/fj/articles/skyhook/skyhook.asp [cited 29 Nov. 2005].

[10]Jun, Y.-W., Hall, K. R., Bennett, A. G., and Bridges, P. D., "Optimal Guidance for Airborne Cable Pickup System," AIAA Paper 84-1893, Aug. 1984.

[11]Huffman, R. R., and Genin, J., "The Dynamical Behaviour of a Flexible Cable in a Uniform Flow Field," *Aeronautical Quarterly*, Vol. 22, May 1971, pp. 183–195.

[12]Phillips, W. H., "Theoretical Analysis of Oscillations of a Towed Cable," NACA TN-1796, Jan. 1949.

[13]Genin, J., Citron, S. J., and Huffman, R. R., "Coupling of Longitudinal and Transverse Motions of a Flexible Cable in a Uniform Flow Field," *Journal of the Acoustical Society of America*, Vol. 52, No. 1, 1972, pp. 438–440.

[14]Norris, S. R., and Andrisani, D., "Longitudinal Equilibrium Solutions for a Towed Aircraft and Tow Cable," AIAA Paper 2001-4254, Aug. 2001.

[15]Nakagawa, N., and Obata, A., "Longitudinal Stability Analysis of Aerial-Towed Systems," *Journal of Aircraft*, Vol. 29, No. 6, 1992, pp. 978–985.

[16]Etkin, B., "Stability of a Towed Body," *Journal of Aircraft*, Vol. 35, No. 2, 1998, pp. 197–205.

[17]Cochran, J. E., Innocenti, M., No., T. S., and Thukral, A., "Dynamics and Control of Maneuverable Towed Flight Vehicles," *Journal of Guidance, Control, and Dynamics*, Vol. 15, No. 5, 1992, pp. 1245–1252.

[18]Henderson, J. F., Potjewyd, J., and Ireland, B., "The Dynamics of an Airborne Towed Target System with Active Control," *Proceedings of the Institution of Mechanical Engineers*, Vol. 213, No. 5, 1999, pp. 305–319.

[19]Bourmistrov, A. S., Hill, R. D., and Riseborough, P., "Nonlinear Control Law for Aerial Towed Target," *Journal of Guidance, Control, and Dynamics*, Vol. 18, No. 6, 1995, pp. 1232–1238.

[20]Quisenberry, J. E., and Arena, A. S., "Dynamic Simulation of Low Altitude Aerial Tow Systems," AIAA Paper 2004-4813, Aug. 2004.

[21]Russell, J. J., and Anderson, W. J., "Equilibrium and Stability of a Circularly Towed Cable Subject to Aerodynamic Drag," *Journal of Aircraft*, Vol. 14, No. 7, 1977, pp. 680–686.

[22]Murray, R. M., "Trajectory Generation for a Towed Cable System Using Differential Flatness," *IFAC World Congress*, Pergamon, New York, 1996, pp. 395–400.

[23]Borst, R. G., Greisz, G. F., and Quynn, A. G., "Fuzzy Logic Control Algorithm for Suppressing E-6A Long Trailing Wire Antenna Wind Shear Induced Oscillations," AIAA Paper 93-3868, Aug. 1993.

[24]Trivailo, P., Sgarioto, D., and Blanksby, C., "Optimal Control of Aerial Tethers for Payload Rendezvous," *The 5th Asian Control Conference*, IEEE Press, Piscataway, NJ, July 2004, pp. 396–404.

[25]Schram, J. W., and Reyle, S. P., "A Three-Dimensional Dynamic Analysis of a Towed System," *Journal of Hydronautics*, Vol. 2, No. 4, 1968, pp. 213–220.

[26]Ablow, C. M., and Schechter, S., "Numerical Simulation of Undersea Cable Dynamics," *Ocean Engineering*, Vol. 10, No. 6, 1983, pp. 443–457.

[27]Roberts, G. M., Connell, H. J., and May, R. L., "A Three Dimensional Model of a Towed Cable-Body System," Dept. of Mathematics, Research Rept. 14, RMIT Univ., Melbourne, Victoria, Australia, Aug. 1994.

[28]Chin, C. K. H., May, R. L., and Connell, H. J., "A Numerical Model of a Towed Cable-Body System," *Journal of the Australian Mathematical Society*, Vol. 42, Pt. E, 2000, pp. C362–C384.

[29]Pai, P. F., and Nayfeh, A. H., "Fully Nonlinear Model of Cables," *AIAA Journal*, Vol. 30, No. 12, 1992, pp. 2993–2996.

[30]No, T. S., and Cochran, J. E., "Dynamics and Control of a Tethered Flight Vehicle," *Journal of Guidance, Control, and Dynamics*, Vol. 18, No. 1, 1995, pp. 66–72.

[31]Leonard, J. W., and Nath, J. H., "Comparison of Finite Element and Lumped Parameter Methods for Oceanic Cables," *Engineering Structures*, Vol. 3, No. 3, 1981, pp. 153–167.

[32]Buckham, B., Nahon, M., and Seto, M., "Three-Dimensional Dynamics Simulation of a Towed Underwater Vehicle," *18th International Conference on Offshore Mechanics and Arctic Engineering*, American Society of Mechanical Engineers, Paper OMAE99/OSU-3068, New York, 1999.

[33]Winget, J. M., and Huston, R. L., "Cable Dynamics—A Finite Segment Approach," *Computers and Structures*, Vol. 6, No. 6, 1976, pp. 475–480.

[34]Kamman, J. W., and Huston, R. L., "Modeling of Variable Length Towed and Tethered Cable Systems," *Journal of Guidance, Control, and Dynamics*, Vol. 22, No. 4, 1999, pp. 602–608.

[35]Dreyer, T. P., and Murray, D. M., "On the Modeling of Two-Dimensional Segmented Representations of Cable Shape," *Ocean Engineering*, Vol. 11, No. 6, 1984, pp. 609–625.

[36]Choo, Y.-I., and Casarella, M. J., "A Survey of Analytical Methods for Dynamic Simulation of Cable-Body Systems," *Journal of Hydronautics*, Vol. 7, No. 4, 1973, pp. 137–144.

[37]Stuart, T. D., Clifton, J. M., and Schmidt, L. V., "Wind-Tunnel Tests of an Inclined Cylinder Having Helical Grooves," *AIAA Journal*, Vol. 33, No. 4, 1995, pp. 665–670.

[38]Every, M. J., King, R., and Weaver, D. S., "Vortex-Induced Vibrations of Cylinders and Cables and Their Suppression," *Ocean Engineering*, Vol. 9, No. 2, 1982, pp. 135–137.

[39]Kane, T. R., Linkins, P. W., and Levinson, D. A., *Spacecraft Dynamics*, McGraw–Hill, New York, 1983, Chap. 4.

[40]Hoerner, S. F., *Fluid-Dynamic Drag*, published by author, 1965, Chap. 3.

[41]Bootle, W., "Forces on an Inclined Circular Cylinder in Supercritical Flow," *AIAA Journal*, Vol. 9, No. 3, 1971, pp. 514–516.

[42]Lorenzini, E. C., Bortolami, S. B., Rupp, C. C., and Angrilli, F., "Control and Flight Performance of Tethered Satellite Small Expendable Deployment System-II," *Journal of Guidance, Control, and Dynamics*, Vol. 19, No. 5, 1996, pp. 1148–1156.

[43]Gill, P. E., Murray, W., and Saunders, M. A., "SNOPT: An SQP Algorithm for Large-Scale Constrained Optimization," *SIAM Journal on Optimization*, Vol. 12, No. 4, 2002, pp. 979–1006.

[44]Williams, P., "User's Guide to DIRECT Version 1.17," Technical Rept. 2005-C-01, Royal Melbourne Inst. of Technology, Melbourne, Australia, March 2005.

[45]Ross, I. M., and Fahroo, F., "Pseudospectral Knotting Methods for Solving Optimal Control Problems," *Journal of Guidance, Control, and Dynamics*, Vol. 27, No. 3, 2004, pp. 397–405.

[46]Williams, P., "Jacobi Pseudospectral Methods for Solving Optimal Control Problems," *Journal of Guidance, Control, and Dynamics*, Vol. 27, No. 2, 2004, pp. 293–297.

[47]Hager, W. W., "Runge–Kutta Methods in Optimal Control and the Transformed Adjoint System," *Numerische Mathematik*, Vol. 87, No. 2, 2000, pp. 247–282.

[48]Betts, J. T., *Practical Methods for Optimal Control Using Nonlinear Programming*, SIAM Press, Philadelphia, 2001, Chap. 3.